Available online at www.sciencedirect.com
SCIENCE DIRECT®
International Journal of Heat and Mass Transfer 47 (2004) 2283–2292
International Journal of HEAT and MASS TRANSFER
www.elsevier.com/locate/ijhmt

# Enhanced heat transfer due to curvature-induced lateral vortices in laminar flows in sinusoidal corrugated-plate channels

H.M. Metwally [a], R.M. Manglik [b,*]

[a] FLUENT Inc., Evanston, IL 60201, USA
[b] Thermal-Fluids and Thermal Processing Laboratory, University of Cincinnati, Cincinnati, OH 45221-0072, USA

Received 10 June 2003; received in revised form 4 November 2003

**Abstract**

Laminar periodically developed forced convection in sinusoidal corrugated-plate channels with uniform wall temperature, and single-phase constant property flows is considered. Numerical solutions are obtained using the control-volume finite-difference method for a wide range of channel corrugation aspect ratios ($0 \leqslant \gamma \leqslant 1$), and flow rates ($10 \leqslant Re \leqslant 1000$) of viscous liquids ($Pr = 5$, 35, and 150). The flow field is found to be strongly influenced by $\gamma$ and $Re$, and it displays two distinct regimes: a low $Re$ or $\gamma$ undisturbed laminar-flow regime, and a high $Re$ or $\gamma$ swirl-flow regime. In the no-swirl regime, the flow behavior is very similar to that in fully developed straight-duct flows with no cross-stream disturbance. In the swirl regime, flow separation and reattachment in the corrugation troughs generates transverse vortex cells that grow spatially with $Re$ and $\gamma$, and the transition to this regime also depends on $Re$ and $\gamma$. The mixing produced by these self-sustained transverse vortices is found to significantly enhance the heat transfer, depending upon $\gamma$, $Re$, and $Pr$, with a relatively small friction factor penalty. The consequent exchanger compactness and heat transfer enhancement effectiveness ($j/f$) is up to 5.5 times that for parallel-plate channels.


## 1. Introduction

Theoretical or experimental results for laminar flow heat transfer in complex and enhanced duct geometries are essential for the design and application of compact heat exchangers [1–3]. Of particular interest for a wide spectrum of usage in food, pharmaceutical, and chemical processing is the plate heat exchanger (PHE) [4–6]. The corrugation patterns on the plate-surfaces of PHEs essentially promote enhanced heat transfer in their inter-plate channels, thereby facilitating small approach temperature operation with a more compact heat exchanger. This is particularly beneficial for processing thermally degradable fluids such as food products, pharmaceutical media, and personal care and biochemical products [5,6].

The most widely used plate-surface pattern in a PHE consists of chevron type corrugations that have a sinusoidal profile [7–9], as shown in Fig. 1. With the chevron inclination (or half included) angle in the range $0° < \beta < 90°$, cross-corrugated channels with multiple metal-to-metal inter-plate point contacts are obtained [6–9]. The case with $\beta = 0°$ yields a set of parallel double-sine-shaped ducts [10] as shown in Fig. 1(b). However, when the chevron inclination angle $\beta = 90°$ in these corrugations, in-phase sinusoidal wavy-plate channels are obtained in the inter-plate flow passages. The peaks and valleys in the top and bottom-plates in this configuration lie on the same longitudinal plane (Fig. 1), with plate spacing equal to twice the waviness amplitude. Also, because the plate spacing $2a$ is much smaller than the plate width $w$, the flow passages can essentially be modeled as two-dimensional wavy-parallel-plate channels,

* Corresponding author. Address: Department of Mechanical, Industrial and Nuclear Engineering, 598 Rhodes Hall, P.O.Box 210072, Cincinnati, OH 45221-0072, USA. Tel.: +1-513-556-5704; fax: +1-513-556-3390.
*E-mail address:* raj.manglik@uc.edu (R.M. Manglik).

0017-9310/$ - see front matter © 2003 Elsevier Ltd. All rights reserved.
doi:10.1016/j.ijheatmasstransfer.2003.11.019

**Nomenclature**

| | |
|---|---|
| $a$ | amplitude of wall waviness |
| $Br$ | Brinkman number |
| $c_p$ | specific heat |
| $f$ | Isothermal Fanning friction factor, Eqs. (8) and (10) |
| $h$ | heat transfer coefficient |
| $j$ | Colburn factor |
| $k$ | thermal conductivity |
| $\dot{m}$ | mass flow rate |
| $Nu$ | Nusselt number, Eqs. (9) and (12b) |
| $p$ | pressure |
| $Pe$ | Peclet number |
| $Pr$ | Prandtl number |
| $q''_w$ | wall heat flux |
| $s$ | developed length of one-wave module of corrugated-plate, Eq. (11) |
| $Re$ | Reynolds number ($\rho u_m 4a/\mu$) |
| $T$ | temperature |
| $\Delta T_{lm}$ | log-mean temperature difference, Eq. (12c) |
| $u$, $v$ | velocity components in the $x$, $y$ directions |
| $w$ | plate width |
| $x$, $y$ | axial and lateral Cartesian coordinates |
| $\alpha$ | thermal diffusivity |
| $\beta$ | included angle in chevron-plate corrugations |
| $\gamma$ | wall corrugation aspect ratio ($4a/\lambda$) |
| $\lambda$ | corrugation half-wave length |
| $\mu$ | dynamic viscosity |
| $\nu$ | kinematic viscosity |
| $\rho$ | density |
| $\tau_w$ | wall shear stress |

*Subscripts*

| | |
|---|---|
| $m$ | bulk or mean value, or period-averaged value |
| $x$ | local value at a given $x$ location |
| w | at the wall or wall conditions |

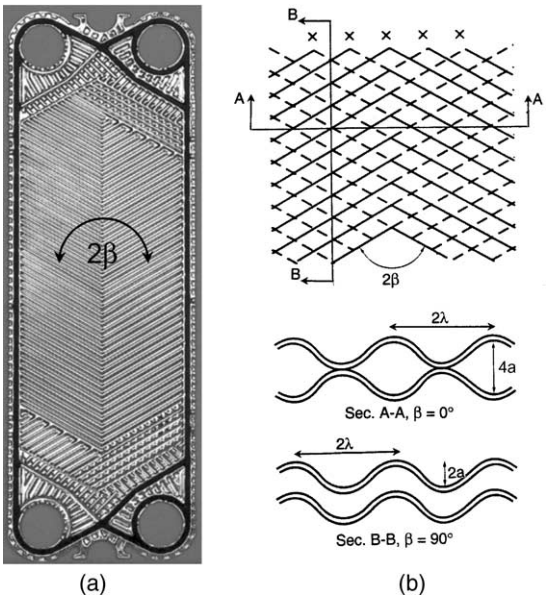


Fig. 1. The flow channel geometry: (a) a typical chevron-plate with sinusoidal corrugations, and (b) inter-plate flow passages.

and this geometry is considered in the present study. The severity of wall waviness is described by its aspect ratio $\gamma$ ($= 4a/\lambda$), where $\gamma = 0$ represents a flat parallel-plate channel.

The flow behavior as well as convective heat transfer and/or mass transport in corrugated-plate channels of different geometrical attributes have been addressed in several studies. The various applications considered in this work include wavy-plate-fin cores [11–15], and dialysis devices and membrane oxygenators [16–20]. Much of this literature, though, deals either with channels where the corrugated walls form converging-diverging flow passages, or in-phase parallel wall corrugations with quite large inter-plate spacing (> twice amplitude of waviness) and/or the walls have sharp corrugations. More recently, attempts have been made to model flows in the cross-corrugated channels of PHEs [6,21,22] for a limited set of duct geometry and flow conditions. The wall waviness has been generally found to promote swirl or vortex flows that result in significant heat and mass transfer enhancement.

Few studies have investigated laminar flow heat transfer in parallel-plate channels with in-phase sinusoidal corrugated walls of the type illustrated in Fig. 1 ($\beta = 90°$ case). Rush et al. [15], Nishimura et al. [18], and Asako et al. [23] have considered the sinusoidal wall geometry, where the plate separation of the wavy channel is quite large. It has been suggested [15,19] that early transition to turbulence might occur at rather moderate Reynolds numbers (<1000). This may perhaps be due to the larger plate spacing ($> 2a$) and a finite duct cross-section aspect ratio [24], and it contradicts other results. The experimental data for inter-plate spacing $= 2a$ as well as the more severe case of cross-corrugated PHE channels suggest steady albeit recirculating or swirl flows for $Re \sim 1000$ [7–9,24–26]. In fact, in some other instances of swirl (curved tube Dean flows, helical channel swirl flows, etc.), the flow has been found to be essentially three-dimensional but steady

with a delayed transition [27–30]. This is further established in the limited set of finite element numerical analysis results of Ektesabi et al. [31] for laminar steady-flow behavior in sinusoidal wavy-plate channels with plate separation in the range $0.667a - 4a$. The flow field is essentially found to be characterized by the onset of lateral vortices in wall corrugation valleys with increasing $Re$, which give rise to substantially higher friction factors than those in flat parallel-plate ducts. However, the heat transfer behavior of viscous liquid flows in such channels and the associated enhancement requires an extended parametric treatment for their effective usage, and this is addressed in this paper.

The objective of this study is to investigate the laminar steady flow and convective heat transfer characteristics of viscous liquids in sinusoidal corrugated parallel-plate channels formed in chevron-plate PHE passages where $\beta = 90°$. The walls are considered to be at uniform temperature, a condition usually encountered in steam heating or refrigerant evaporation cooling of single-phase viscous liquids. Numerical solutions are obtained to study the effects of channel geometry, described by the corrugation aspect ratio range $0 \leqslant \gamma \leqslant 1.0$, flow Reynolds number ($10 \leqslant Re \leqslant 1000$), and fluid Prandtl number ($Pr = 5$, 35, and 150) on the flow fields, local wall shear stresses, temperature distributions, local variations in the wall heat fluxes, and the concomitant friction factors, Nusselt numbers, and the relative heat transfer enhancement.

## 2. Problem formulation and numerical solution

For the sinusoidally corrugated parallel-plate channel geometry and reference coordinate system described in Fig. 2(a), constant property, periodically developed, steady laminar flows of viscous Newtonian fluids with heat transfer are considered. With in-phase wall waviness, the plate separation in the channel is twice the amplitude of the sinusoidal corrugation, i.e., valleys of the top-plate and peaks of the bottom-plate coincide on the mid-plane. This plate gap appropriately models the inter-plate channels in a PHE with chevron-plates where $\beta = 90°$ (see Fig. 1). The duct walls are maintained at a constant temperature (**T** or UWT boundary condition), and axial conduction ($Pe \gg 1$) and viscous dissipation ($Br \ll 1$) are neglected. Furthermore, in ducts with periodically varying flow cross-section or wall geometry in the streamwise direction, the concept of periodically developed flow, as treated by Patankar et al. [32] for example, is applicable. This makes use of the periodicity characteristics of the velocity components, and essentially confines the flow-field analysis to a single corrugation module ($2\lambda$) in the streamwise direction. The temperature field likewise, when normalized by the local bulk fluid temperature, has periodicity characteristics as well.

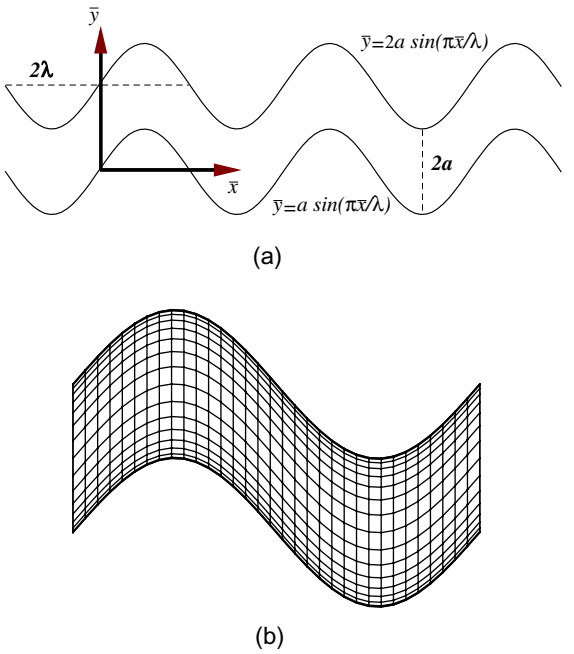


Fig. 2. Parallel-plate channel with in-phase sinusoidal wall waviness: (a) physical domain, and (b) typical grid description in the one-period computational domain.

Thus, for the two-dimensional convection in the wavy channel, the governing equations for mass, momentum, and energy conservation can be expressed as

$$\frac{\partial u}{\partial x} + \frac{\partial u}{\partial y} = 0 \tag{1}$$

$$u\frac{\partial u}{\partial x} + v\frac{\partial u}{\partial y} = -\frac{\partial p}{\partial x} + \nu\left(\frac{\partial^2 u}{\partial x^2} + \frac{\partial^2 u}{\partial y^2}\right) \tag{2a}$$

$$u\frac{\partial v}{\partial x} + v\frac{\partial v}{\partial y} = -\frac{\partial p}{\partial y} + \nu\left(\frac{\partial^2 v}{\partial x^2} + \frac{\partial^2 v}{\partial y^2}\right) \tag{2b}$$

$$u\frac{\partial T}{\partial x} + v\frac{\partial T}{\partial y} = \alpha\left(\frac{\partial^2 T}{\partial x^2} + \frac{\partial^2 T}{\partial y^2}\right) \tag{3}$$

These are subject to the following no slip, uniform wall temperature, and periodicity boundary conditions, respectively:

$$u = v = 0, \quad @y = a\sin(\pi x/\lambda) \text{ and } y = 2a + a\sin(\pi x/\lambda) \tag{4a}$$

$$T = T_w, \quad @y = a\sin(\pi x/\lambda) \text{ and } y = 2a + a\sin(\pi x/\lambda) \tag{4b}$$

$$u(x) = u(x + 2\lambda), \quad v(x) = v(x + 2\lambda), \text{ and } (T/T_m)(x) = (T/T_m)(x + 2\lambda) \tag{4c}$$

From the periodically developed velocity distribution, on the basis of the velocity component tangential to the boundary and its derivative normal to the boundary (or the normalized gradient: $(\partial\phi/\partial n) = \nabla\phi \cdot \hat{n}$), the local wall shear stress can then be calculated from

$$\tau_{w,x} = -\mu[1 + (\pi\gamma/2)^2 \cos^2(\pi x/\lambda)]^{-1}(\partial u/\partial y)|_w \quad (5)$$

Likewise, the local wall heat flux is given by

$$q''_{w,x} = -k[1 + (\pi\gamma/2)^2 \cos^2(\pi x/\lambda)]^{-1/2}(\partial T/\partial y)|_w \quad (6)$$

The average flow velocity $u_m$ and the bulk-mean temperature $T_m$ are, respectively, obtained from their standard definitions as

$$u_m = (1/2a)\int_0^{2a} u\,dy \text{ and } T_m = (1/2au_m)\int_0^{2a} uT\,dy \quad (7a,b)$$

Given the local velocity field, wall shear stress, temperature distribution, and wall heat flux, the local friction factor and Nusselt number are, respectively, given by

$$f_x = [2\tau_{w,x}/(\rho u_m^2)] \quad (8)$$

$$Nu_x = (h_x 4a/k) = [4aq''_{w,x}/k(T_w - T_m)] \quad (9)$$

Correspondingly, the period-integrated overall friction factor is determined from a force balance over the $(2\lambda)$–flow module of Fig. 2(a). This yields

$$f = (2\tau_{w,m}/\rho u_m^2) = (1/\lambda\rho u_m^2)\int_s \tau_{w,x}\,ds \quad (10)$$

Here, though the local wall shear stress is integrated over the actual wavy length $s$ of the plate channel given by

$$s = \int_0^{2\lambda} [1 + (\pi\gamma/2)^2 \cos^2(\pi x/\lambda)]^{1/2}\,dx \quad (11)$$

the friction factor is represented in terms of the projected unit-width plate-surface area $(= 4\lambda)$, i.e., it is based on the surface area of the equivalent flat-plate channel. Similarly, in order to calculate the period-averaged overall Nusselt number, based on the projected heat transfer surface area, the energy balance over the $(2\lambda)$–duct length is invoked to yield the average wall heat flux

$$q''_{w,m} = (1/\lambda)\int_s q''_{w,x}\,ds = (\dot{m}c_p/4\lambda)(T_{m,x+2\lambda} - T_{m,x}) \quad (12a)$$

Thus, from the rate equation based on the log-mean temperature difference, the overall Nusselt number is obtained as

$$Nu = (q''_{w,m} 4a/k\Delta T_{lm}) \quad (12b)$$

where

$$\Delta T_{lm} = \frac{(T_w - T_{m,x}) - (T_w - T_{m,x+2\lambda})}{\ln[(T_w - T_{m,x})/(T_w - T_{m,x+2\lambda})]} \quad (12c)$$

Equations (1)–(3) were solved numerically by using standard finite-difference methods that employ control-volume-based discretization techniques along with a pressure-correction algorithm. For the computations, a non-orthogonal grid as shown in Fig. 2(b) represented the flow domain for the periodic module of axial length $(2\lambda)$. Solutions were obtained with the $(x \times y)$ mesh ranging from $120\times41$ $(\gamma \leqslant 0.25)$ to $120\times81$ $(\gamma = 1.0)$. These grid sizes were fixed by establishing grid independence of the numerical solutions in a few test cases, where there was less than one-percent change in the results with successive mesh refinement. For example, with the more severe case of $\gamma = 1.0$ and $Re = 500$ the change in $f$ when the grid was refined from $120\times81$ to $140\times81$ was less than 0.5%; similarly, the change from $120\times81$ to $120\times91$ was less than 0.4%. Another typical set of grid-refinement results are presented in Fig. 3. The iteration convergence criterion for all computations, represented by the relative magnitude of error

$$\varepsilon = |(\phi^n - \phi^{n-1})/\phi^n| \quad (13a)$$

was set, respectively for the velocity $(\varepsilon_u, \varepsilon_v)$, pressure $(\varepsilon_p)$, and temperature $(\varepsilon_T)$ fields, as

$$\varepsilon_V = \sum(\varepsilon_u + \varepsilon_v + \varepsilon_p) \leqslant 10^{-4}, \text{ and } \varepsilon_T \leqslant 10^{-6} \quad (13b)$$

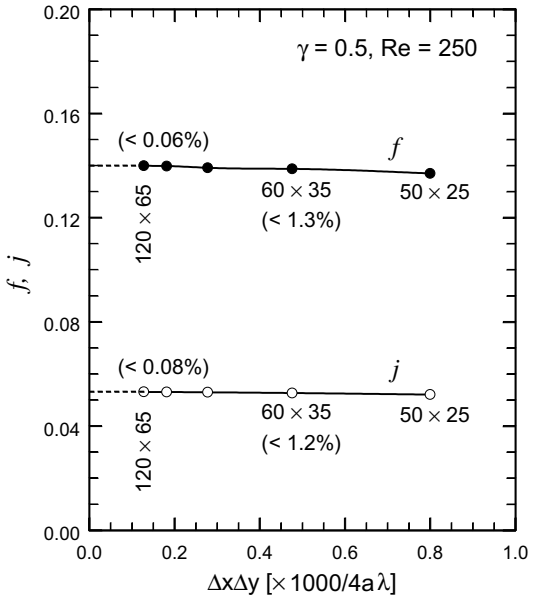


Fig. 3. Typical $(x \times y)$ mesh-refinement results to establish the relative grid insensitivity and accuracy of computations.

Also, the numerical integrations for the wall shear stress, sinusoidal wall length, and wall heat flux were performed using the trapezoidal rule, and second-order accurate differencing schemes were employed to determine the wall derivatives of velocity and temperature. Additional details of the numerical solutions and their validation are given in Ref. [33].

## 3. Results and discussion

### 3.1. Flow distribution and friction factor

As seen in Fig. 4, variations in the pitch and amplitude of the sinusoidal plate-surface corrugations (represented by $\gamma$) and the flow rate (represented by $Re$) have a significant effect on the dynamic behavior of the flow field. The change in flow structure for a fixed flow rate ($Re = 300$) with varying severity of the corrugated-plate-surface waviness is depicted in Fig. 4(a), and the strong influence of the duct geometry on the stream function distribution is evident. With increasing corrugation aspect ratio $\gamma$ (increasing amplitude $a$ or decreasing pitch $\lambda$), fluid re-circulation or swirl flows are generated in the corrugation troughs. The intensity and flow area coverage of this counter-rotating lateral vortex grows with $\gamma$, which in turn lends to higher momentum transfer. Increasing flow $Re$ also produces a similar effect in a channel with fixed corrugation geometry ($\gamma = 0.5$), as displayed by the stream function distribution in Fig. 4(b), where the vortex cell is seen to grow with $Re$. With both increasing $\gamma$ and $Re$, the flow separation point preceding the onset of re-circulation moves upstream toward the peak of the plate-surface corrugation, and the concomitant flow re-attachment point moves further downstream on the oblique face of the wavy wall. At very low Reynolds number ($Re \leqslant O[10]$), or with small-plate waviness ($\gamma < 0.375$), on the other hand, the surface geometry has no effect on the flow, and the fluid moves undisturbed through the channel with no re-circulation by simply "adopting" the wavy passage shape.

The variations in the normalized local wall shear stress ($\tau_{w,x}/\tau_{w,m}$) with $Re$ and $\gamma$ are graphed in Fig. 5. At low flow rates ($Re = 10$) in a channel with $\gamma = 0.5$, there is very little change in the local shear stress along the length of the duct; the small undulations seen in Fig. 5(a) result from local core velocity variations as the flow adapts to the wavy wall contours. As $Re$ increases, however, the shear stress distribution clearly reflects the influence of the wavy-wall trough-region lateral vortex and its streamwise growth. The profile shows a wall-velocity gradient peak at the part of wall exposed to flow acceleration (i.e., the side opposite the trough and flow re-circulation therein). Also, the longitudinal size of the re-circulation bubble can be estimated from the points of separation and reattachment, or zero wall shear stress

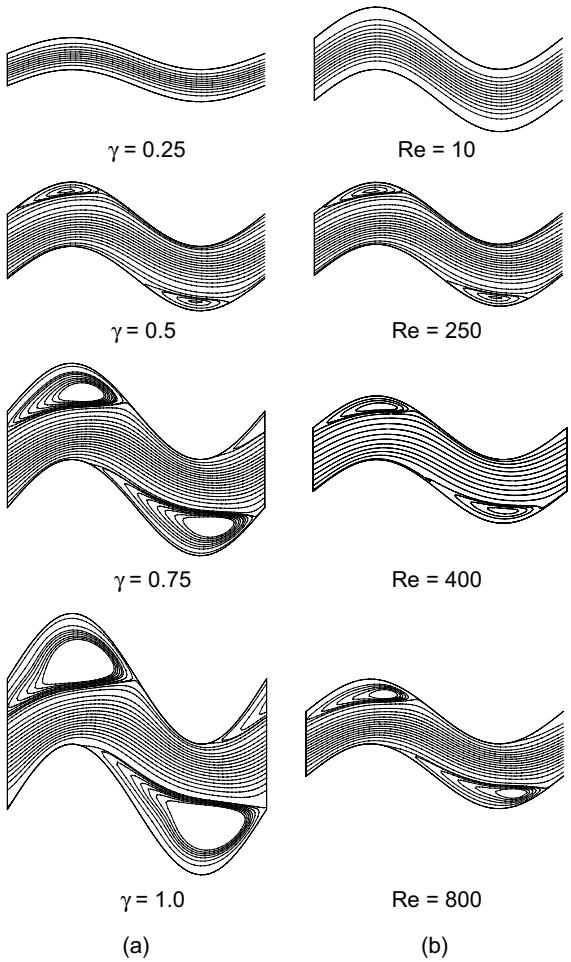


Fig. 4. Streamline distributions in steady laminar flows in sinusoidal corrugated-plate channels: (a) effect of corrugation severity with $0.25 \leqslant \gamma \leqslant 1.0$ and $Re = 300$, and (b) effect of flow rate with $\gamma = 0.5$ and $10 \leqslant Re \leqslant 800$.

locations. A similar behavior is observed in flows with a fixed $Re$ but increasing severity of plate-surface corrugation $\gamma$ in Fig. 5(b). The shear stress again increases with $\gamma$, has a local maximum value in the flow acceleration region, and the flow separation and reattachment points (upstream and downstream ends of the wall trough) that encapsulate the lateral swirl.

The effects of the duct geometry (as described by $\gamma$) on the flow frictional losses are seen in Fig. 6, where results for the changes in the isothermal Fanning friction factor $f$ with $Re$ are graphed for $0.25 \leqslant \gamma \leqslant 1.0$. Also included is the well-known result for flow in a flat parallel-plate channel ($f = 24/Re$), which corresponds to fully developed laminar flow in the reference case of $\gamma = 0$. It is evident that higher frictional losses are incurred with increasing severity of the plate corrugation

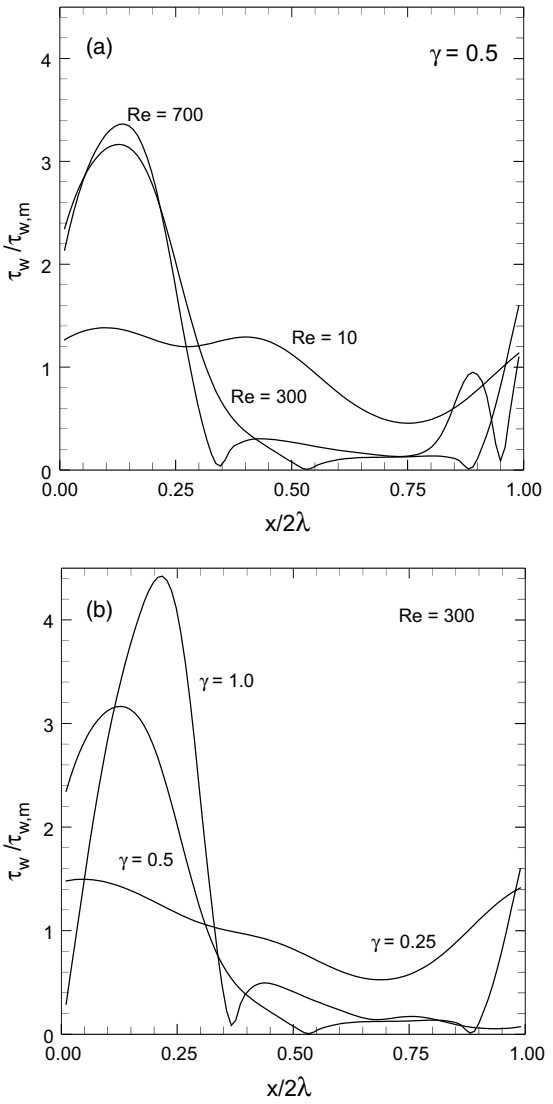


Fig. 5. Local wall shear stress distribution in steady laminar flows in sinusoidal wavy-plate channels: (a) effect of flow *Re*, and (b) effect of channel wall waviness.

($\gamma > 0 \rightarrow 1$). Also seen is the influence of the onset of swirl flow in the troughs of the wall corrugation on $f$, which is depicted by the deviation from the log-linear behavior of ($f - Re$) at higher Reynolds number in each $\gamma$ case. As pointed out earlier, the increased friction factor in this regime is predominantly due to the onset and growth of lateral vortices in the channel troughs that enhance fluid momentum transfer thereby increasing the wall shear stress. In the low Reynolds number regime, however, where (*fRe*) is constant, the increase in the frictional loss with $\gamma$ is primarily due to the increased effective flow length or surface area. For example, corrugated-plates with $\gamma = 0.5$ have a 14% larger effective

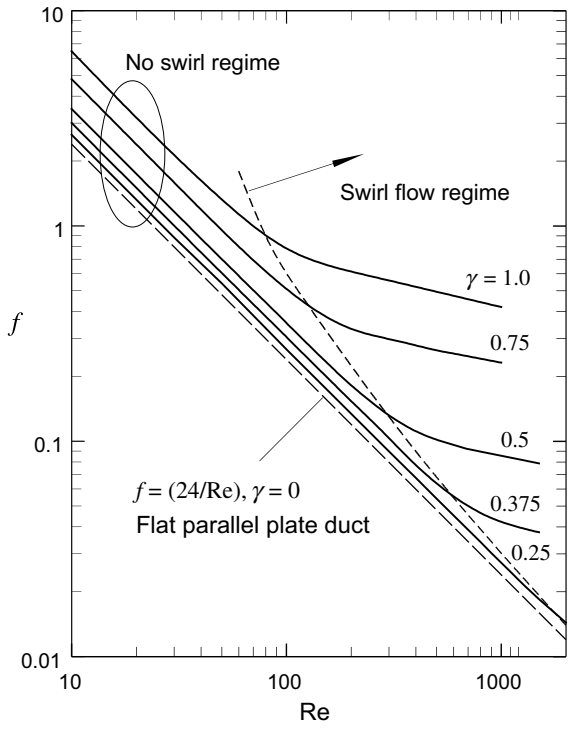


Fig. 6. Laminar flow Isothermal Fanning friction factors in sinusoidally corrugated parallel-plate channels.

length (or 28% higher surface area per unit width of the plate pair) as compared to flat-plates.

The inter-play of channel-plate-surface geometry and flow distribution, reflected in the wall shear stress distributions and friction factor results, clearly suggests that the flow can be categorized into two distinct regimes: (1) an undisturbed streamline flow regime, and (2) a steady swirl-flow regime that is characterized by self-sustained transverse vortices in the wall trough regions. This demarcation is graphically shown in the $f - Re$ plots of Fig. 6. A general critical Reynolds number, however, does not seem to uniquely represent the transition from one regime to the other, and it is different for each channel of different corrugation aspect ratio $\gamma$.

### 3.2. Temperature distribution and Nusselt number

The temperature distributions in Fig. 7 atypically depict the enhanced laminar forced convection heat transfer due to the wall corrugations and the swirl flows they induce. The periodically developed temperature fields under constant wall temperature (**T** or UWT) conditions for a viscous liquid with $Pr = 35$ are graphed. With the growth of transverse vortices in the wall troughs, which encompass much of the bulk flow field

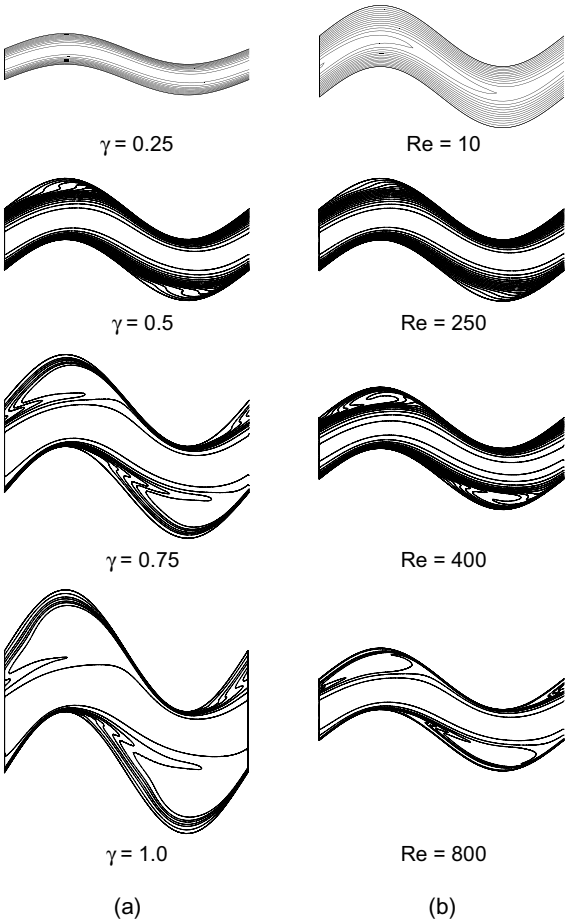


Fig. 7. Temperature distributions in steady laminar viscous liquid ($Pr = 35$) flows in sinusoidal corrugated-plate channels: (a) effect of corrugation severity with $0.25 \leqslant \gamma \leqslant 1.0$ and $Re = 300$, and (b) effect of flow rate with $\gamma = 0.5$ and $10 \leqslant Re \leqslant 800$.

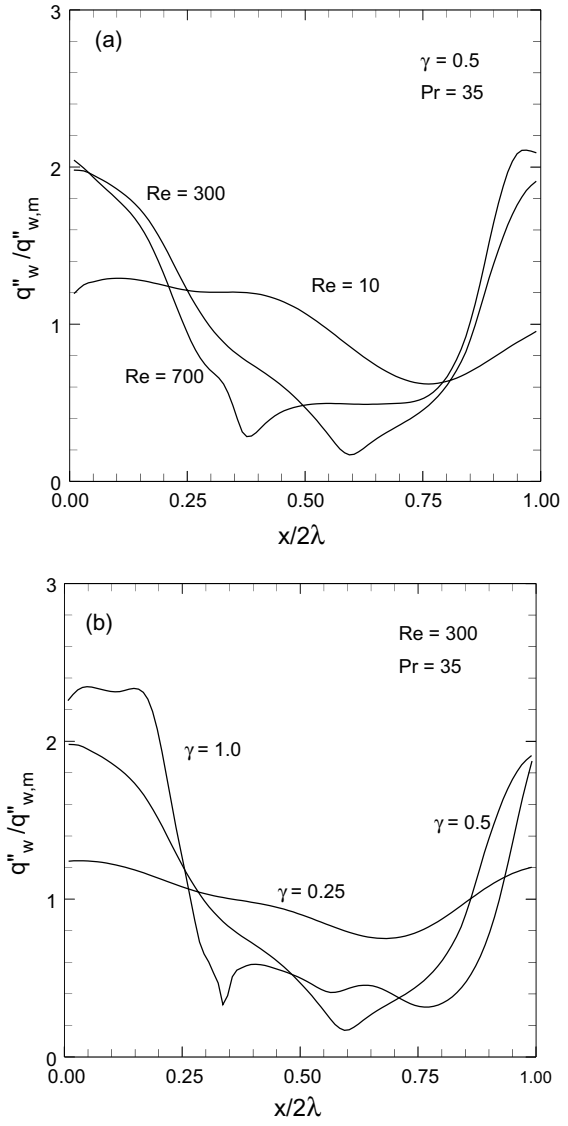


Fig. 8. Local wall heat flux distribution in steady laminar flows in sinusoidal wavy-plate channels: (a) effect of flow *Re*, and (b) effect of channel wall waviness.

with increasing $\gamma$, the convective transport is enhanced substantially, as seen from the isotherm maps of Fig. 7(a). There is considerable thinning of the thermal boundary layer with higher wall temperature gradients as $\gamma = 0.25 \rightarrow 1.0$. This behavior is also evident in Fig. 7(b), where the local wall temperature gradients are seen to increase with flow rate ($Re = 10 \rightarrow 800$) in the channel with $\gamma = 0.5$. Once again, the onset and growth of swirl flows promotes a more uniform temperature field with sharper wall gradients thereby enhancing the convective heat transfer.

The influence of swirl on heat transfer is further seen in Fig. 8, where the variation in the local wall heat flux, normalized by its mean value over the one-period duct length ($q''_{w,x}/q''_{w,m}$), virtually mimics the normalized local wall shear stress behavior. As the swirl develops and grows in the wall troughs of a channel with fixed $\gamma(= 0.5)$ and increasing *Re*, large variations in ($q''_{w,x}/q''_{w,m}$) are seen, with peak values at the wall exposed to flow acceleration on the side opposite the re-circulation zone (Fig. 8(a)). A relatively larger impact on the local heat transfer enhancement is perhaps due to increasing duct corrugation aspect ratio $\gamma$ as seen in Fig. 8(b), where considerably higher local peak heat fluxes are obtained as $\gamma \rightarrow 1$; the level of deterioration in the re-circulation region decreases somewhat and is more than offset by the larger peak values. With low *Re* flows or less severe corrugation (low $\gamma$) channels, however, the local heat flux remains virtually constant with small changes due to local fluid acceleration caused by wall undulations.

That the transverse vortices induced in the troughs of the plate-surface corrugations promote enhanced convection in the flow cross-section and increase the overall or mean heat transfer coefficient is clearly evident from Fig. 9. In this figure, the variation in Nusselt number with Reynolds number for a highly viscous liquid ($Pr = 150$) and different corrugation aspect ratio $\gamma$ is presented. Relative to the performance of the parallel-plate channel in fully developed laminar flow with constant wall temperature conditions ($Nu = 7.541$), the heat transfer coefficient in corrugated channels is enhanced several folds, depending upon $\gamma$ and $Re$. The largest increase in the period-averaged Nusselt number is obtained with higher $\gamma$ and $Re$, or the swirl flow regime. With $\gamma = 1.0$ and $Re = 1000$, for example, $Nu$ is 34 times higher than that in a parallel-plate channel. Furthermore, similar to the $f - Re$ behavior seen in Fig. 6, the effect of swirl on $Nu$ also diminishes as $Re$ and/or $\gamma$ decreases. The higher heat transfer coefficients in the no-swirl regime are once again due to the larger surface area of corrugated channels.

Moreover, the effect of fluid Prandtl number on the temperature field is depicted by the isotherms graphed in Fig. 10. Three different values of $Pr$ (5, 35, and 150) are considered, which are representative of most viscous liquids encountered in thermal processing applications, with $Re = 200$ and $\gamma = 1.0$. The improved convective behavior with increasing $Pr$ is clearly evident, where

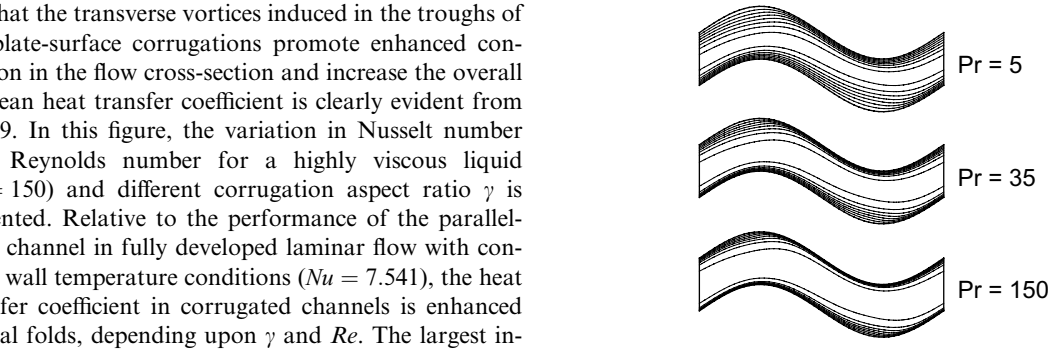


Fig. 10. Variation in temperature distribution with fluid Prandtl number ($5 \leqslant Pr \leqslant 150$) in flows in a wavy channel with $\gamma = 0.5$ and $Re = 200$.

higher temperature gradients at the wall are obtained. With low $Pr$ fluids the temperature distribution is relatively more stratified, whereas at high $Pr$ it tends to be more uniform. This is also seen in Fig. 11, where higher Nusselt numbers are obtained in higher Prandtl number fluids. With a typical $Re = 700$ flow rate, for example, which corresponds to the periodically developed swirl flow regime for $\gamma = 0.5$, $Nu$ ($Pr = 35$) is 99% higher than $Nu$ ($Pr = 5$). The corresponding enhancement in $Nu$ for $Pr = 150$ over that for $Pr = 35$ and the same flow rate is 77%. Another notable feature of the results in Figs. 9 and 11 is that the surface area enlargement in the non-swirl regime has a relatively greater impact on enhancing heat transfer, compared to its effect on flow frictional loss (Fig. 6).

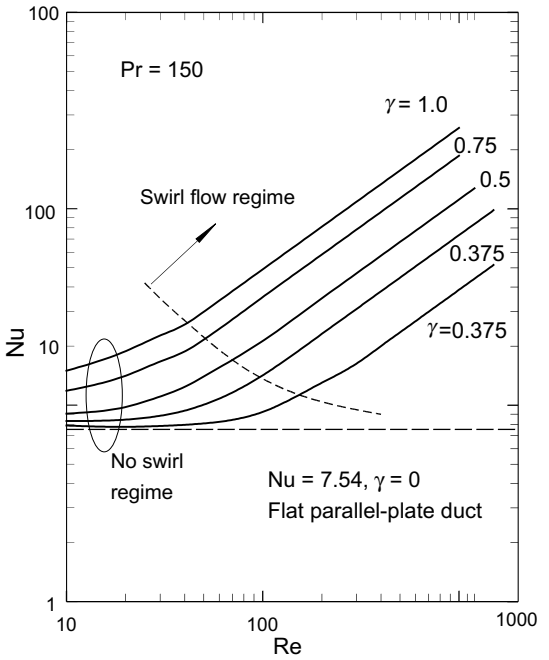


Fig. 9. Viscous fluid ($Pr = 150$) laminar flow Nusselt numbers in sinusoidally corrugated parallel-plate channels with uniform wall temperature.

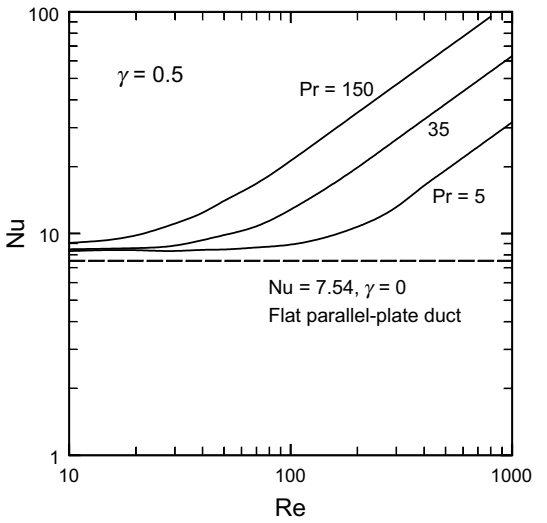


Fig. 11. Effect of Prandtl number on variation of Nusselt number with laminar flow Reynolds number in a wavy-plate channel with $\gamma = 0.5$ and uniform wall temperature.

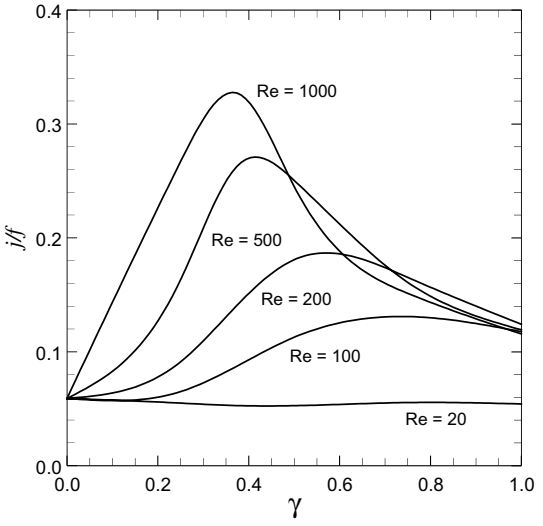


Fig. 12. Evaluation of laminar flow heat transfer enhancement in sinusoidal corrugated-plate channels with uniform wall temperature on the basis of the area goodness ($j/f$) factor.

Given that the improvements in heat transfer are also accompanied by increases in the frictional losses, it is necessary to evaluate the net enhancement obtained in the wavy-plate channels. One way of assessing the relative thermal-hydraulic performance enhancement, among many others [1–3,34] is to consider the *area goodness factor* [34] given by

$$(j/f) = (Nu\ Pr^{-1/3}/fRe) \tag{14}$$

Here, $j(= Nu/Re\ Pr^{1/3})$ is the Colburn factor, and the measure seeks to evaluate the free-flow area (and hence the frontal area) requirements of a compact heat exchanger. The results for this figure of merit are graphed in Fig. 12 for $0 \leqslant \gamma \leqslant 1$, where, it may be noted that, $\gamma = 0$ represents a flat parallel-plate channel. The optimum performance relative to the plate corrugation aspect ratio $\gamma$ is seen to be a function of Reynolds number. Less severe waviness is seen to perform better with high flow rates. On the other hand with very low flow rates ($Re \sim O[20]$ or less), the surface corrugations do not offer any performance enhancement over a flat-plate channel. For flow rates that generally correspond to the swirl regime ($Re > O[1\,0\,0]$), considerable enhancement is obtained and plate-surface corrugations with $0.3 \geqslant \gamma \geqslant 0.6$ provide the greatest advantage.

## 4. Conclusions

Numerical solutions for laminar ($10 < Re < 1000$), incompressible, single-phase, periodically developed, constant property, forced convection in sinusoidal corrugated-plate channels maintained at uniform wall temperature are obtained. Results for a wide range of channel corrugation aspect ratio ($0 < \gamma < 1.0$), and for viscous liquids represented by three values of Prandtl number (5, 35, and 150) are considered. The plate-surface corrugations essentially generate transverse vortices in their trough regions, and this re-circulation is seen to grow with increasing $\gamma$ and $Re$. The inception and growth of steady swirl and the concomitant periodic disruption and thinning of the boundary layer promote enhanced transport of heat as well as momentum. In this swirl-flow dominated regime, depending upon $\gamma$, $Re$, and $Pr$, the heat transfer is found to be enhanced by up to 34 times that in a flat parallel-plate channel ($Pr = 150$ fluid), whereas the corresponding friction factor penalty is only 18 times higher. The optimum ($j/f$) performance is obtained for corrugation geometries in the range $0.3 \leqslant \gamma \leqslant 0.6$. In the non-swirl flow regime, the enlarged surface area of the corrugated-plate is solely responsible for the enhancement, and the thermal benefits are significantly less.

It maybe noted, however, that acquisition of controlled and extended experimental data, which are not available at present, would greatly help in corroborating the computational observations in this study. Also, the influence of temperature-dependent property variations needs further investigation, and these are envisaged in a continuation of this work.

## Acknowledgements

This study was supported in part by the National Science Foundation (Grant # CTS-9502128), and the UERP Grant from The Procter & Gamble Co.

## References

[1] R.L. Webb, Principles of Enhanced Heat Transfer, Wiley, New York, 1994.
[2] A.E. Bergles, Techniques to enhance heat transfer, in: W.M. Rohsenow, J.P. Hartnett, Y.I. Cho (Eds.), Handbook of Heat Transfer, third ed., McGraw-Hill, New York, 1998 (Chapter 11).
[3] R.M. Manglik, Heat transfer enhancement, in: A. Bejan, A.D. Kraus (Eds.), Heat Transfer Handbook, Wiley, New York, 2003 (Chapter 14).
[4] R.K. Shah, W.W. Focke, Plate heat exchangers and their design theory, in: R.K. Shah, E.C. Subbarao, R.A. Mashelkar (Eds.), Heat Transfer Equipment Design, Hemisphere, New York, 1988, pp. 227–254.
[5] R.M. Manglik, Plate heat exchangers for process industry applications: Enhanced thermal-hydraulic characteristics of chevron-plates, in: R.M. Manglik, A.D. Kraus (Eds.), Process, Enhanced and Multiphase Heat Transfer, Begell House, New York, 1996, pp. 267–276.

[6] L. Wang, B. Sundén, R.M. Manglik, Plate Heat Exchangers: Design, Applications, and Performance, W.I.T. Press, Southampton, UK, in press.
[7] W.W. Focke, J. Zachariades, I. Olivier, The effect of the corrugation inclination angle on the thermohydraulic performance of plate heat exchangers, Int. J. Heat Mass Transfer 28 (8) (1985) 1469–1479.
[8] A. Muley, R.M. Manglik, Experimental study of turbulent flow heat transfer and pressure drop in a plate heat exchanger with chevron plates, J. Heat Transfer 121 (1) (1999) 110–117.
[9] A. Muley, R.M. Manglik, H.M. Metwally, Enhanced heat transfer characteristics of viscous liquid flows in a chevron-plate heat exchanger, J. Heat Transfer 121 (4) (1999) 1011–1017.
[10] R.M. Manglik, J. Ding, Laminar flow heat transfer to viscous power-law fluids in double-sine ducts, Int. J. Heat Mass Transfer 40 (6) (1997) 1379–1390.
[11] J.E. O'Brien, E.M. Sparrow, Corrugated-duct heat transfer, pressure drop, and flow visualization, J. Heat Transfer 104 (1982) 410–416.
[12] Y. Asako, M. Faghri, Finite-volume solution for laminar flow and heat transfer in a corrugated duct, J. Heat Transfer 109 (1987) 627–634.
[13] V.K. Garg, P.K. Maji, Flow and heat transfer in a sinusoidally curved channel, Int. J. Eng. Fluid Mech. 1 (3) (1988) 293–319.
[14] L.C. Yang, Y. Asako, Y. Yamaguchi, M. Faghri, Numerical prediction of transitional characteristics of flow and heat transfer in a corrugated duct, J. Heat Transfer 119 (1) (1997) 62–69.
[15] T.A. Rush, T.A. Newell, A.M. Jacobi, An experimental study of flow and heat transfer in sinusoidal wavy passages, Int. J. Heat Mass Transfer 42 (1999) 1541–1553.
[16] B.J. Bellhouse, F.H. Bellhouse, C.M. Curl, T.I. MacMillan, A.J. Gunning, E.H. Spratt, S.B. MacMurung, J.M. Nelems, A high efficiency membrane oxygenator and pulsatile pumping system, and its application to animal trials, Trans. Am. Soc. Artificial Internal Organs 19 (1973) 72–78.
[17] T. Nishimura, Y. Ohori, Y. Kajmoto, Y. Kawamura, Mass transfer characteristics in a channel with symmetric wavy wall for steady flow, J. Chem. Eng. Jpn. 18 (6) (1985) 550–555.
[18] T. Nishimura, Y. Kajimoto, Y. Kawamura, Mass transfer enhancement in channels with wavy walls, J. Chem. Eng. Jpn. 19 (2) (1986) 142–144.
[19] T. Nishimura, K. Yano, T. Yoshino, Y. Kawamura, Occurrence and structure of Taylor-Goertler vortices induced in two-dimensional wavy channels for steady flow, J. Chem. Eng. Jpn. 23 (6) (1990) 697–703.
[20] T. Nishimura, S. Murakami, S. Arakawa, Y. Kawamura, Flow observations and mass transfer characteristics in symmetrical wavy-walled channels at moderate Reynolds numbers for steady flow, Int. J. Heat Mass Transfer 33 (5) (1990) 835–845.
[21] M. Ciafalo, J. Stasiek, M.W. Collins, Investigation of flow and heat transfer in corrugated passages II. Numerical simulation, Int. J. Heat Mass Transfer 39 (1) (1996) 165–192.
[22] D.R. Sawyers, M. Sen, H.-C. Chang, Heat transfer enhancement in three-dimensional corrugated channel flow, Int. J. Heat Mass Transfer 41 (1998) 3559–3573.
[23] Y. Asako, H. Nakamura, M. Faghri, Heat transfer and pressure drop characteristics in a corrugated duct with rounded corners, Int. J. Heat Mass Transfer 31 (1988) 1237–1244.
[24] P. Gschwind, A. Regele, V. Kottke, Sinusoidal wavy channels with Taylor-Goertler vortices, Exp. Therm. Fluid Sci. 11 (1995) 270–275.
[25] D. Béreiziat, R. Devienne, M. Lebouché, Local flow structure for non-Newtonian fluids in a periodically corrugated wall channel, J. Enhanced Heat Transfer 2 (1–2) (1995) 71–77.
[26] C. Zimmer, P. Gschwind, G. Gaiser, V. Kottke, Comparison of heat and mass transfer in different heat exchanger geometries with corrugated walls, Exp. Therm. Fluid Sci. 26 (2002) 269–273.
[27] K.R. Sreenivasan, P.J. Strykowski, Stabilization effects in flow through helically coiled pipes, Exp. Fluids 1 (1983) 31–36.
[28] J. Hart, J. Ellenberger, P.J. Hamersma, Single- and two-phase flow through helically coiled tubes, Chem. Eng. Sci. 43 (4) (1988) 775–783.
[29] R.M. Manglik, S. Maramraju, A.E. Bergles, The scaling and correlation of low Reynolds number swirl flows and friction factors in circular tubes with twisted-tape inserts, J. Enhanced Heat Transfer 8 (6) (2001) 383–395, pp. 183–266.
[30] R.M. Manglik, A.E. Bergles, Swirl flow heat transfer and pressure drop with twisted-tape inserts, Advances in Heat Transfer, 36, Academic Press, New York, NY, 2002.
[31] M.R.M. Ektesabi, M. Sako, T. Chiba, Fluid flow and heat transfer in wavy sinusoidal channels (1st Report, numerical analysis of two dimensional laminar flow field), Nippon Kikai Gakkai Ronbunshu Bhen, Trans. JSME, 53 (487) (1987) 722–730.
[32] S.V. Patankar, C.H. Liu, E.M. Sparrow, Fully developed flow and heat transfer in ducts having streamwise-periodic variations of cross-sectional area, J. Heat Transfer 99 (1977) 180–186.
[33] H.M. Metwally, R. M. Manglik, A computational study of enhanced laminar forced convection heat transfer to Newtonian and non-Newtonian fluid flows in sinusoidal corrugated-plate channels, Thermal-Fluids and Thermal Processing Laboratory Report No. TFTPL-6, University of Cincinnati, July 2002.
[34] R.K. Shah, A.L. London, in: . In: Laminar forced convection in ducts, in: T.F. Irvine Jr., J.P. Hartnett (Eds.), Advances in Heat Transfer, Academic, New York, 1978 (Suppl. 1).